

# Numerical and Experimental Investigations on Mach 2 and 4 Pseudo-Shock Waves in a Square Duct

By Liquan SUN, Hiromu SUGIYAMA, Kazuhide MIZOBATA, Ryojiro MINATO and Akira TOJO

*Department of Mechanical Systems Engineering, Muroran Institute of Technology, Muroran, Japan*

(Received August 8th, 2003)

The structures and characteristics of  $\lambda$ -shaped and X-shaped pseudo-shocks in a square duct are investigated through numerical simulations and experiments at Mach 2 and Mach 4, respectively. The experiments were carried out in a pressure-vacuum supersonic wind tunnel with a test cross section of  $80 \times 80 \text{ mm}^2$ . Numerical simulations were carried out using the Harten-Yee second-order TVD scheme and the Baldwin-Lomax turbulence model. The Reynolds numbers for the Mach 2 and 4 cases were  $Re_\infty = 2.53 \times 10^7$  and  $Re_\infty = 2.36 \times 10^7$ , respectively, and the flow confinement was  $\delta_\infty/h = 0.35$  for both cases. The computational results for the Mach 2 pseudo-shock wave are in good agreement with the experimental results. Based on this agreement, the flow quantities, which are very difficult to obtain experimentally, were analyzed by numerical simulation. Although several differences were found between the computational results and experiments in the case of Mach 4 due to asymmetric characteristics in experiment which could not be reproduced in numerical simulation, the computational results are valuable for understanding this complex asymmetric phenomenon.

**Key Words:** Pseudo-Shock Wave, Supersonic Flow, Shock Wave/Turbulent Boundary Layer Interaction, Shock Train, Numerical Simulation

## 1. Introduction

When a supersonic flow is decelerated to subsonic flow in a duct, a very complicated multiple shock wave system and highly nonuniform flow, involving a shock train, shear layer and separation region, are produced as a result of interaction between the shock wave and the duct wall turbulent boundary layer. The multiple shock wave system and resulting mixing region construct a pseudo-shock wave (PSW),<sup>1)</sup> which plays a role similar to that of a single normal shock. Unlike the case in external flow, such as flow around flying bodies, wings and missiles, PSW often occurs in devices such as scramjet engines/combustor-isolators, scramjet inlets, supersonic wind tunnel diffusers and supersonic ejectors, and affects the performance and efficiency of these devices significantly. Therefore, study of the PSW is very important in engineering applications. Several researchers have investigated the structure and characteristics of the PSW experimentally, including Ikui et al.,<sup>2)</sup> Sugiyama et al.<sup>3–6)</sup> and Carroll and Dutton,<sup>7)</sup> and through numerical simulations, for example Hataue,<sup>8)</sup> Carroll et al.<sup>9)</sup> and Yamane et al.<sup>10)</sup> However, several important flow quantities of the PSW could not be measured via experimental methods, and numerical simulations have not agreed well with the experimental findings. Therefore, the detailed structure, characteristics, and turbulence phenomena of the PSW have not been fully clarified. Moreover, the Mach number in most of these previous studies was lower than 2. For research on supersonic and hypersonic air breathing propulsion, study of the PSW at higher Mach numbers is increasingly important.

The structure of the PSW is mainly influenced by the up-

stream Mach number of the main flow and flow confinement, as described by the ratio of the undisturbed boundary layer thickness upstream of the PSW to the duct half-height. In a previous paper,<sup>11)</sup> by producing a PSW at upstream and mid-stream locations in a Mach 2 supersonic square duct, the present authors investigated the relationship between the flow confinement, structure, and characteristics of the PSW in a duct at the same Mach number by high-speed color schlieren visualization and wall pressure measurements. The detailed velocity and pressure distributions, as well as the effect of flow confinement on the structure and characteristics of the Mach 2 PSW, were also analyzed by numerical simulation. In the present paper, using a supersonic wind tunnel and numerical simulations, the detailed structures and characteristics of Mach 2 and Mach 4 PSWs with the same flow confinement are investigated. The numerical results are then compared with the experimental results to evaluate the accuracy of the numerical predictions.

## 2. Experimental Apparatus and Method

Figure 1 shows a schematic diagram of the pressure-vacuum intermittent supersonic wind tunnel<sup>6)</sup> employed in the present study. Two-dimensional symmetric supersonic nozzles of flow Mach number  $M = 1.96$  and  $3.98$  were used. The maximum working times of the wind tunnel were 15 s and 20 s under the Mach 2 and 4 conditions, respectively. Figure 2 shows a schematic diagram of the test section. The length and cross section of the test section were 1500 mm and  $80 \times 80 \text{ mm}^2$ . The structures of the PSW were visualized using a high-speed color schlieren system with a nanospark flash (30 ns) light source. The wall pressures were

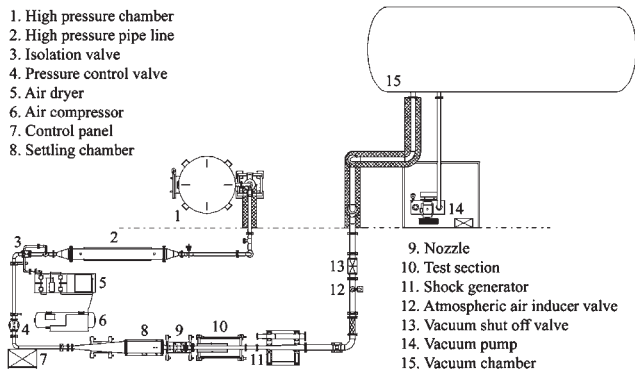


Fig. 1. Pressure-vacuum supersonic wind tunnel.

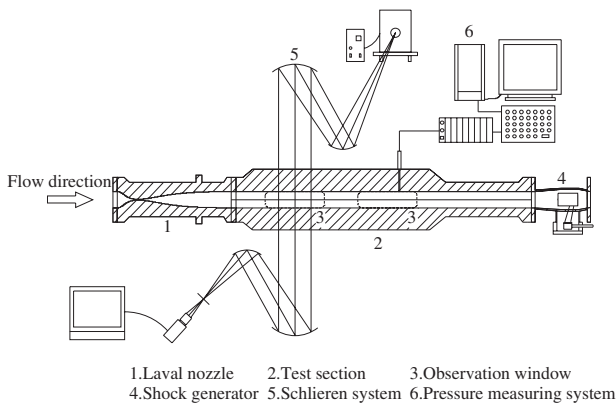


Fig. 2. Test section and measuring system.

measured at 43 points along the centerline of the upper wall of the test section duct using pressure transducers. Two-dimensional Laval nozzles and the square duct with a relatively large cross section make the flow in the test section close to a two-dimensional flow, especially at the central part of the duct.

**3. Numerical Method**

To clarify the flows near the central part of the square duct, time-averaged, two-dimensional Navier-Stokes equations are used as governing equations, which are described in reference 11). The Harten-Yee second-order upwind total variation diminishing (TVD) scheme<sup>12)</sup> and central difference are used to solve the convection terms and viscous terms of the equations, respectively. A second-order fractional step procedure is applied to obtain a solution for the time term. The laminar viscosity is obtained using the Sutherland viscosity law, and the Baldwin-Lomax algebraic turbulence model<sup>13)</sup> is used as the first step of numerical investigations for the present PSW flows.

The initial condition is given by setting an inviscid normal shock at the rear of the computational region. The inlet condition is set uniform across the mainflow, and the boundary layer velocity profile is given by a 1/7-power-law. As the outflow boundary condition, density and velocity are obtained from a one-point extrapolation and the value of pressure is determined from the experimental result. At the duct

Table 1. Flow conditions.

	Mach 2	Mach 4
Flow confinement	0.35	0.35
Reynolds number	$2.53 \times 10^7$	$2.36 \times 10^7$
Stagnation pressure	196 kPa	490 kPa
Stagnation temperature	300 K	300 K

centerline, the symmetric quantities are obtained from a second-point extrapolation. Adiabatic, no-slip, solid wall boundary conditions are applied at the wall of the duct. The flow conditions are described in Table 1.

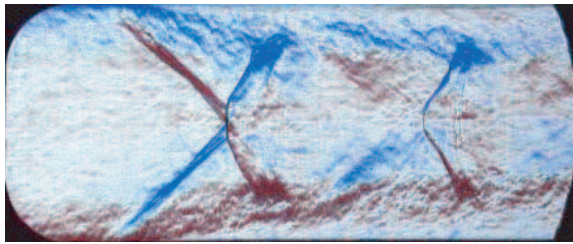
The grid comprises 865 points in the streamwise direction at equal intervals, and 73 points in the transverse direction at unequal intervals in order to resolve the behavior of the turbulent boundary layer near the wall. The computational region is the central part of the duct, with length 12 times the height of the duct, and only one half of the duct is computed. The grid systems of  $1729 \times 73$ ,  $865 \times 145$  and  $1729 \times 145$  are used to verify the effect of grid density on the numerical results. Although sharper shock waves and finer structures of the PSW can be captured using finer grid systems, there are no obvious differences in the general structures.

**4. Results and Discussion**

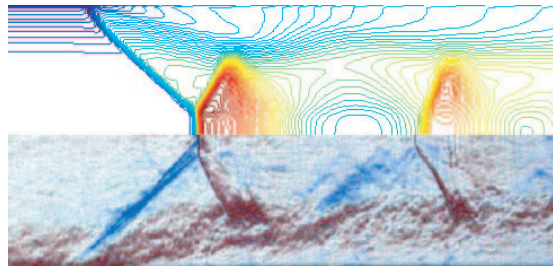
**4.1. Structures of the Mach 2 and Mach 4 pseudo-shock waves**

Figure 3(a) shows a high-speed color schlieren photograph for the Mach 2 experiment. The flow direction is from left to right. From this figure, the bifurcated first shock wave can be clearly observed as the λ-shaped first shock wave, with a vertical portion, two front legs, two rear legs and two bifurcation points (refer to Fig. 7(c)). The secondary shock is unbifurcated and is concave facing downstream with a nearly normal outer region. At the foot of the first shock wave, the boundary layer separates from the wall and the boundary layer thickness increases continuously. Figure 3(b) shows a comparison of the numerical results with the schlieren photograph by inserting computed density contours in the upper half of the figure. It can be seen that the calculated shape and structure of the first and second shock waves, the spacing between the first and second shock wave, and the change in the turbulent boundary layer, match the schlieren photograph very well.

Similarly, Figs. 4(a) and (b) show the results for the Mach 4 PSW. It can be seen from Fig. 4 that with increasing Mach number, the shape of the first shock changes from λ-shaped to X-shaped, that is, there is no vertical portion in the first shock wave and the two front legs intersect directly at one point (refer to Fig. 8(c)). In Fig. 4(a), the first shock has an asymmetric oblique shock pattern. The bottom front shock originates from the bottom wall upstream of the location where the front shock originates from the top wall, such that the two front shocks intersect above the centerline and the main flow inclines toward the top wall. In fact, the shock system sometimes attaches to the bottom wall and some-

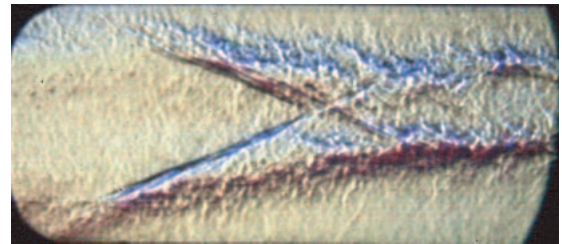


(a) Schlieren photograph.

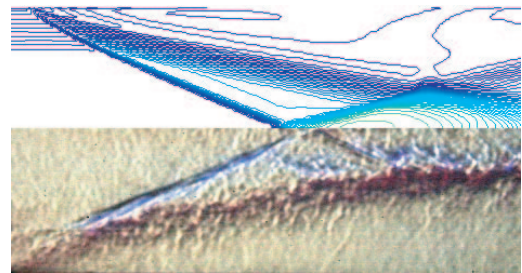


(b) Comparison of schlieren photograph and density contours (CFD).

Fig. 3. Schlieren photograph and density contours (CFD) of the Mach 2 pseudo-shock wave.

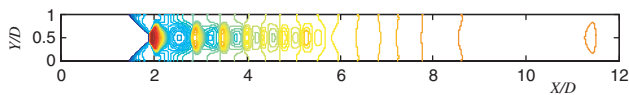


(a) Schlieren photograph.

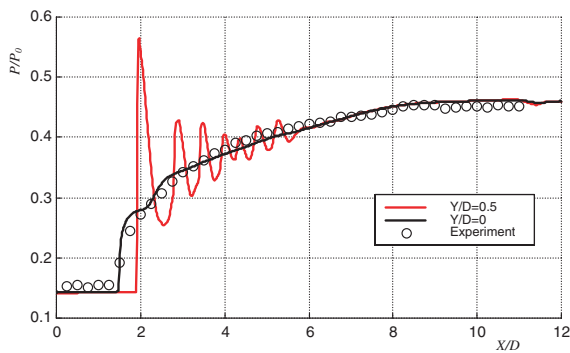


(b) Comparison of schlieren photograph and density contours (CFD).

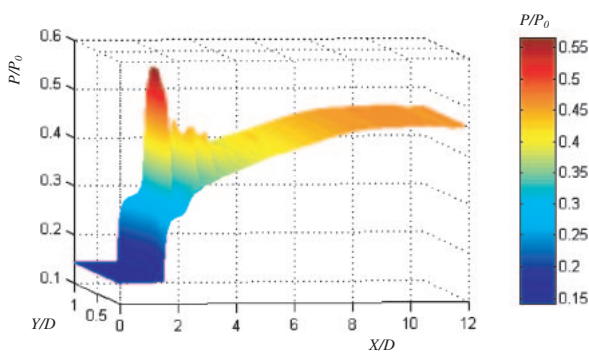
Fig. 4. Schlieren photograph and density contours (CFD) of the Mach 4 pseudo-shock wave.



(a) Static pressure contours.

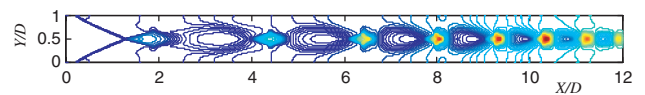


(b) Static pressure distributions.

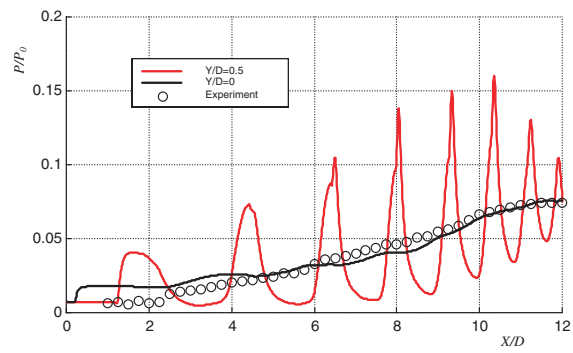


(c) Static pressure distribution on the center plane of the duct.

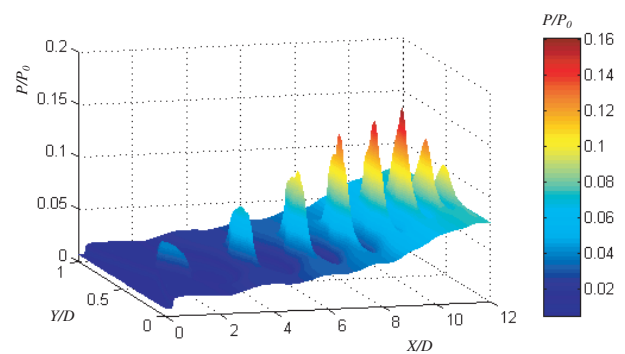
Fig. 5. Static pressure distribution for the Mach 2 pseudo-shock wave.



(a) Static pressure contours.



(b) Static pressure distributions.



(c) Static pressure distribution on the center plane of the duct.

Fig. 6. Static pressure distribution for the Mach 4 pseudo-shock wave.

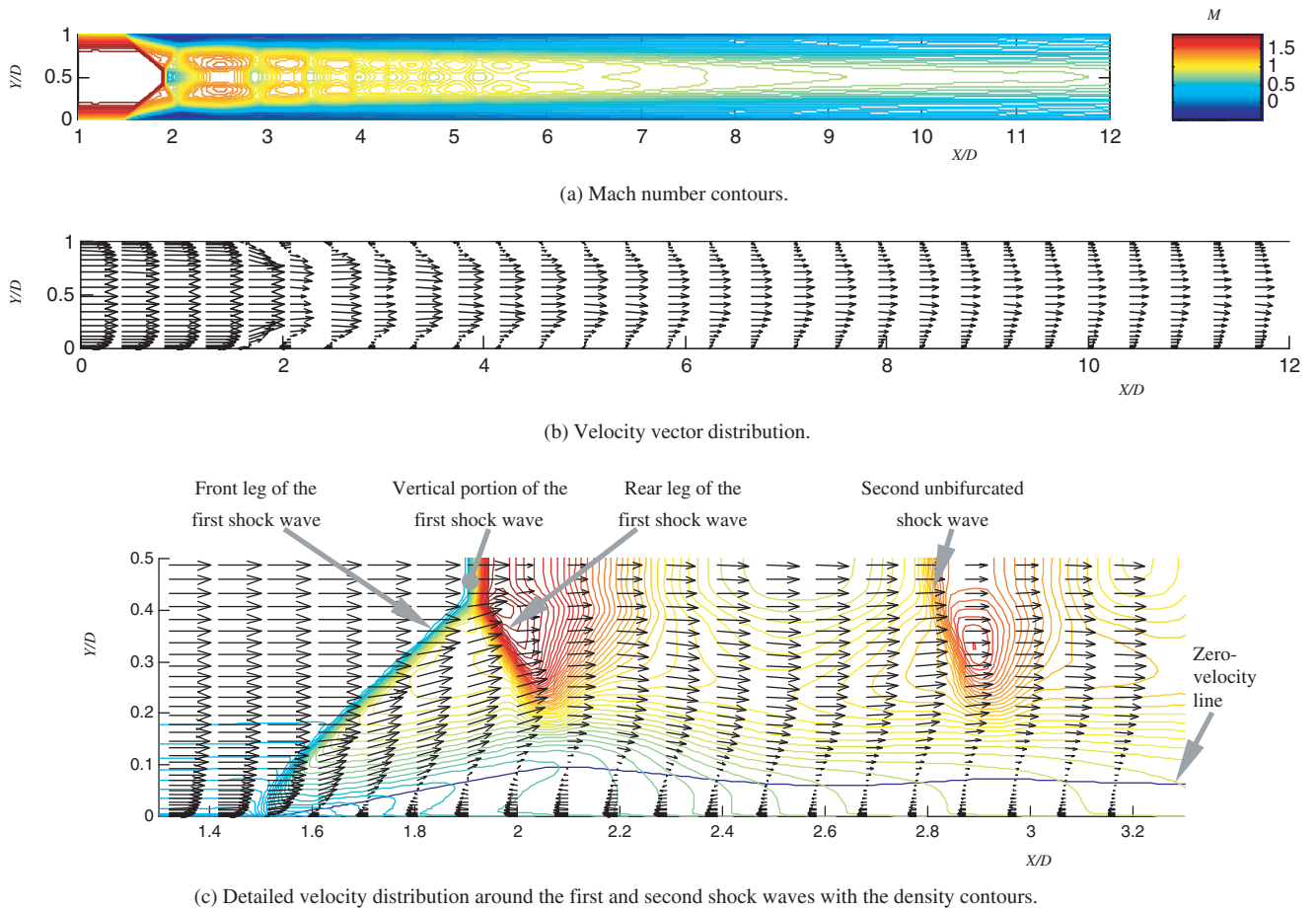


Fig. 7. Mach number contours and velocity vector distribution for the Mach 2 pseudo-shock wave.

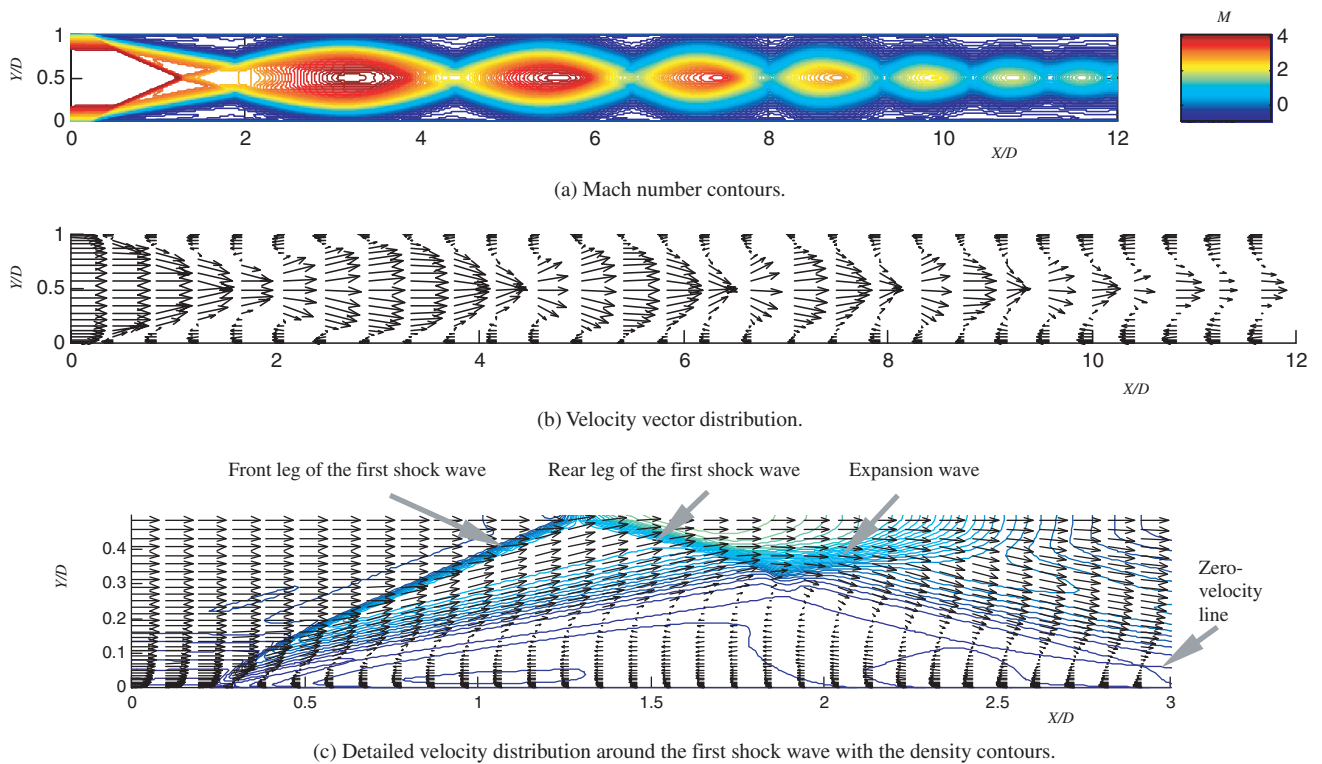


Fig. 8. Mach number contours and velocity vector distribution for the Mach 4 pseudo-shock wave.

times attaches to the top wall randomly in experiments. Similar asymmetric trends of X-shaped PSWs were observed by Carroll and Dutton<sup>7)</sup> at Mach 2.45. A considerably large amplification in the scale of the turbulence structure can be observed under the first shock wave. Moreover, two types of unsteadiness in the case of Mach 4 were observed in the high-speed digital video images. The first feature was a high-frequency streamwise oscillation, and the second was a transverse oscillation appearing at the location of the intersection point, oscillating in the transverse direction. The maximum amplitude of the streamwise oscillation was about 0.7 times the height of the duct. However, the two kinds of oscillation were minor at Mach 2. Although the oscillation of the PSW is beyond the scope of this paper, it is one of the possible reasons for discrepancy between the numerical results and experimental results in the wall static pressure distribution in the case of the Mach 4 PSW, as will be discussed in section 4.2.

As the mechanism and cause of this asymmetric phenomenon have not been fully clarified, numerical simulations were conducted assuming symmetric flow. A comparison of the lower half of the schlieren photograph and computed density contours is shown in Fig. 4(b). The angle between the front leg of the first shock and the duct wall, the structure of the first shock, the large scale of the boundary layer separation, and the change in the turbulent boundary layer, all match that half of the schlieren photograph well.

#### 4.2. Static pressure distributions of the Mach 2 and Mach 4 pseudo-shock waves

Figure 5(a) shows the computed static pressure contours indicating the position of shocks in the shock train, and Fig. 5(b) shows the static pressure distributions along the duct obtained by the numerical simulation and experiment for Mach 2 conditions. The solid black line represents the numerical result, and the black circles represent the experimental result for the wall pressure distribution. The horizontal axis in Fig. 5(b) denotes the distance  $X$  from the computational region entrance, normalized by the height of the duct  $D$ , and the vertical axis represents the static pressure  $P$ , normalized by the stagnation pressure  $P_0$  in the upstream settling chamber. Figure 5(b) shows that the wall pressure initially rises rapidly due to the first shock wave, and continues to rise moderately thereafter. The computation predicts the magnitude of the measured wall pressure distribution very accurately. The curve of the static pressure distribution along the centerline of the duct in Fig. 5(b) shows that the pressure increase due to the first shock is larger and steeper than due to successive shocks, and at the end of the shock train, the static pressure at the center of the duct is equal to that at the wall. The pressure recovery through the shock train is about 79% of an ideal normal shock value.

Figure 5(c) shows the full details of the static pressure distribution on the center plane of the duct. It is seen that except for the first shock, the increase in static pressure induced by successive shock is saddle-shaped. Therefore, the pressure increase induced by the outer portion near the edge of the boundary layer is stronger than that induced

by the center portion of the shock. This tendency is similar to that reported in a previous paper<sup>14)</sup> for a flow confinement of  $\delta_\infty/h = 0.25$  and Mach 2 conditions.

Figure 6 shows the static pressure distributions for the Mach 4 PSW under the assumption of symmetric flow. The coordinates in each figure correspond to those in Fig. 5. From Fig. 6(a), it can be seen that the spacing between each shock is longer than that for the Mach 2 PSW, indicating that longer spacing between shocks may be characteristic of higher Mach numbers. Figure 6(b) shows that the static pressure distribution on the centerline of the duct is different from that at Mach 2 in that the maximum pressure rise is induced by successive shocks, not the first shock wave. The pressure rise induced by each shock wave increases gradually downstream up to a peak, and then decreases gradually. Similar characteristics for X-shaped PSWs were reported by Tamaki et al.,<sup>15)</sup> Yamane et al.<sup>10)</sup> and Lin et al.<sup>16)</sup> Comparing the computed static wall pressure distribution with the experimental result, it can be observed that the shape of pressure recovery on the wall is well reproduced by the present numerical simulation, but the length of pressure recovery is longer than that in the experiment by about two times the height of the duct. The reason for this difference is considered to be the symmetric flow assumption of the numerical simulation, as well as the strong oscillation of the PSW. The turbulence model adopted in the present study may therefore not be entirely suitable for high Mach number PSWs. The pressure recovery through the shock train in this case is about 55%, lower than that of an ideal normal shock value. The reduction in static pressure rise in comparison with the ideal normal shock may result from the existence of the upstream boundary layer, wall friction, turbulence mixing loss inside the PSW, or existence of reverse flow. Comparing the cases of Mach 2 and Mach 4, the increase in Mach number appears to induce greater static pressure loss. The reason for this is considered to be stronger compression and expansion of flow in the case of the Mach 4 PSW, with a much larger reverse flow region. Related discussions are given in the next section.

Figure 6(c) shows the details of the static pressure distribution on the center plane of the duct. The stronger pressure fluctuation can be observed, and the peaks in pressure induced by each shock wave are distributed on the centerline of the duct, very different from the saddle-shaped profile obtained for the Mach 2 PSW.

#### 4.3. Velocity distributions of the Mach 2 and Mach 4 pseudo-shock waves

Figures 7(a) and (b) show the Mach number contours and velocity vector distribution for the Mach 2 PSW. The flow immediately outside the boundary layer behind each shock remains supersonic, known as a supersonic tongue. The core flow behind each shock becomes subsonic and then reaccelerates to become supersonic before the next shock appears, resulting in the saddle-shaped velocity cross-sections in the shock train region. The flow immediately behind the shock train is mixed supersonic near the outer edge of the boundary layer and subsonic in the core region, and is referred to

here as the mixing region. In this region, as the low-speed flow extends to the center of the duct, the entire flow is gradually decelerated to become subsonic, and the velocity profiles change from trapezoidal behind the shock train to parabolic in the latter half of the mixing region. A successive increase in the boundary layer thickness is observed passing through this interaction.

The expanded velocity vector distribution around the first and second shocks in the lower half of the duct is shown in Fig. 7(c), together with the density contours, to indicate the position of the shocks. The blue line in the figure represents the zero-velocity line. The direction of the velocity changes toward the center due to the front leg of the first shock, and toward the wall after the rear leg. Similar processes occur after each successive shock, gradually weakening in the downstream direction. This tendency agrees well with the experimental results reported in a previous paper<sup>4)</sup> by Sugiyama et al. concerning the velocity profile measured by laser Doppler velocimetry (LDV) under a Mach 1.83 condition. The boundary layer separates at the foot of the front leg of the first shock. A large separation region about 4 times the height of the duct is predicted by the present numerical simulation, and a recirculation flow appears between the rear leg of the first shock and the duct wall.

Figures 8(a), (b) and (c) show the Mach number contours, velocity vector distribution, and expanded velocity vector distribution around the first shock wave in the lower half of the duct for the Mach 4 PSW. Except for the boundary layer, no subsonic flow or supersonic tongue is observed behind any of the shock waves. The decrease in flow speed due to the first shock wave is small, and the spacing between successive shocks decreases through interaction, with later shock waves becoming more obscure (except for the first oblique shock wave). These characteristics agree well with the experimental results reported in a previous paper,<sup>17)</sup> concerning a velocity profile measured by particle image velocimetry (PIV) under the same Mach 4 condition. The directions of flow velocities first change toward the center of the duct due to the first oblique shock wave, and then toward the wall. Similar processes occur through each successive shock, gradually weakening in the downstream direction. There is no mixing region as observed for the Mach 2 PSW. The speed of the core flow at the duct end is still supersonic, at about Mach 2. Similar characteristics were reported by Lin et al.<sup>16)</sup> for the Mach 3 condition. In Fig. 8(c), three waves including one front oblique shock wave, one rear oblique shock wave and one expansion wave can be observed. The boundary layer separates largely at the foot of the front leg of the first shock, and a large recirculation region appears between the three waves and the duct wall. The large reverse flow and intense compression and expansion in the case of the Mach 4 PSW may be the reason for the smaller static pressure recovery than in the case of the Mach 2 PSW.

From Fig. 8(b), the present numerical simulation is confirmed to predict the reverse flow through whole duct. However, unfortunately, the separation length measured through

oil flow visualization in a previous study<sup>18)</sup> shows that the separation lengths at the top and bottom walls are about 1.5 times and 4 times the height of the duct, respectively, although the oscillation of the PSW and the thickness of the oil may affect the accuracy of visualization. However, the numerical result may help explain why the X-shaped PSW is always asymmetric. As is well known, the reverse flow affects the steadiness of the flow, and tends to be restrained by flow or by confinement such as a wall. Under asymmetric flow, the separation region becomes smaller, and the flow becomes much steadier. Further experimental and numerical analyses will be needed to obtain a full understanding of this ambiguous phenomenon.

## 5. Conclusions

Numerical simulations and experiments of Mach 2 and Mach 4 PSWs with the same flow confinement in a square duct were conducted. Simulations were based on two-dimensional Navier-Stokes equations with a Baldwin-Lomax turbulence model, and experiments were conducted in a pressure-vacuum intermittent supersonic wind tunnel.

Schlieren photographs and density contours obtained through numerical simulations clarified the detailed structures of these PSWs. At Mach 2, the first shock wave is  $\lambda$ -shaped, and the successive shock waves are unbifurcated, concaving toward the upstream direction and weakening gradually downstream. The boundary layer begins to separate at the foot of the front leg of the first shock wave, and the boundary layer thickness increases gradually downstream. In the case of Mach 4, an asymmetric X-shaped PSW and large separation of the boundary layer were observed experimentally. As the mechanism for this asymmetry was unclear, numerical simulations were performed assuming symmetric flow. Comparison of the computed density contours of the first shock wave in the lower half of the section with schlieren photograph revealed that the structure of the first shock wave and the changes of the turbulent boundary layer obtained by numerical simulation are roughly in agreement with the experiments.

The wall pressure distribution obtained by numerical simulation was in reasonable agreement with the experimental results for the Mach 2 PSW. In this case, the static pressure increases induced by successive shock waves have saddle-shaped profiles, except for the first shock, which produces the maximum static pressure increase. At Mach 4, the static pressure peaks are distributed along the centerline of the duct, and the maximum static pressure increase is induced by a successive shock wave.

The direction of flow velocities changes toward the center from the foot of the first shock front leg and then toward the wall in both cases, repeating in the downstream direction. However, the change in flow direction is more pronounced at Mach 4. The general patterns of velocity profiles through the duct differ between these two flow conditions. The Mach number contours reveal that the center flow at the outlet of the duct is still supersonic in the case of Mach 4, yet be-

comes subsonic in the case of Mach 2. The reverse flow through the whole interaction region was predicted by numerical simulation at Mach 4 but this does not agree with experimental result, due to the simplified assumption of symmetric flow. Possible reasons for the higher stability of the asymmetric flow compared to symmetric flow in the case of the X-shaped PSW at Mach 4 were suggested.

The present simulation adequately reproduced the structure and characteristic of the Mach 2  $\lambda$ -shaped PSW, and modeled certain important features of the Mach 4 X-shaped PSW. Although there are several discrepancies between the numerical results and experimental results in the case of the Mach 4 PSW, the numerical results provide valuable insight into the asymmetric phenomenon of X-shaped PSWs, serving as a first step toward the understanding the PSW at higher Mach numbers.

### References

- 1) Matsuo, K., Miyazato, Y. and Kim, H. D.: Shock Train and Pseudo-Shock Phenomena in Internal Gas Flows, *Progress in Aerospace Sciences*, **35** (1999), pp. 33–100.
- 2) Ikui, T., Matsuo, K. and Nagai, M.: The Mechanism of Pseudo-Shock Waves, *Bull. JSME*, **17** (1974), pp. 731–739.
- 3) Sugiyama, H., Takeda, H., Zhang, J. P., Okuda, K. and Yamagishi, H.: Locations and Oscillation Phenomena of Pseudo-Shock Waves in a Straight Rectangular Duct, *JSME Int. J. Ser. II*, **31** (1988), pp. 9–15.
- 4) Sugiyama, H., Arai, T. and Uno, N.: LDV Investigation of Turbulence Phenomena in Multiple Shock Wave/Turbulent Boundary Layer Interactions, Proc. of IUTAM Symp. on Combustion in Supersonic Flows, Champion, M. and Deshaies, B. (eds.), Kluwer Academic Publishers, 1995, pp. 325–332.
- 5) Sugiyama, H., Arai, T. and Kagawa, T.: Multiple Shock Wave/Turbulent Boundary Layer Interactions and Turbulence Phenomena in a Supersonic Rectangular Duct, Proc. of 4th KSME-JSME Fluids Eng. Conf., 1998, pp. 25–28.
- 6) Sugiyama, H., Fukuda, K., Mizobata, K., Endo, K., Sun, L. Q. and Arai, T.: Study on Supersonic Internal Flows with Shock Waves (Development of the Experimental Apparatus for Supersonic Internal Flows and Characteristics of the Pseudo-Shock Waves in Mach 2 and 4 Internal Flows), *Trans. JSME*, **68** (2002), pp. 3295–3301 (in Japanese).
- 7) Carroll, B. F. and Dutton, J. C.: Characteristics of Multiple Shock Wave/Turbulent Boundary-Layer Interactions in Rectangular Ducts, *J. Propul. Power*, **6** (1990), pp. 186–193.
- 8) Hataue, I.: Computational Study of the Shock-Wave/Boundary-Layer Interaction in a Duct, *Fluid Dynam. Res.*, **5** (1989), pp. 217–234.
- 9) Carroll, B. F., Lopez-Fernandez, P. A. and Dutton, J. C.: Computations and Experiments for a Multiple Normal Shock/Boundary-Layer Interaction, *J. Propul. Power*, **9** (1993), pp. 405–411.
- 10) Yamane, R., Oshima, S., Nakamura, Y., Ishii, T. and Park, M. K.: Numerical Simulation of Pseudoshock in Straight Channels, *JSME Int. J. Ser. B*, **38** (1995), pp. 549–554.
- 11) Sun, L. Q., Sugiyama, H., Mizobata, K. and Fukuda, K.: Numerical and Experimental Investigations on the Mach 2 Pseudo-Shock Wave in a Square Duct, *J. Visualization*, **6** (2003), pp. 363–370.
- 12) Yee, H. C.: A Class of High-Resolution Explicit and Implicit Shock-Capturing Methods, NASA TM, 101088, 1989.
- 13) Baldwin, B. S. and Lomax, H.: Thin Layer Approximation and Algebraic Model for Separated Flows, AIAA Paper 78-257, 1978.
- 14) Sun, L. Q., Sugiyama, H., Mizobata, K., Fukuda, K. and Hiroshima, T.: Study on Supersonic Internal Flows with Shock Waves (Investigations by Numerical Analysis on the Internal Structure of Mach 2 Pseudo-Shock Wave in a Two-Dimensional Channel), *Trans. JSME*, **69** (2003), pp. 772–778 (in Japanese).
- 15) Tamaki, T., Tomita, Y. and Yamane, R.: A Study of Pseudo-Shock, 2nd Report, X-type Pseudo-Shock, *Bull JSME*, **14** (1971), pp. 807–817.
- 16) Lin, P., Rao, G. V. R. and O'Connor, G. M.: Numerical Investigation on Shock Wave/Boundary-Layer Interactions in a Constant Area Diffuser at Mach 3, AIAA Paper 91-1766, 1991.
- 17) Fukuda, K., Sugiyama, H., Mizobata, K., Endo, K., Sun, L. Q. and Hiroshima, T.: Study on Supersonic Internal Flows with Shock Waves (Experiments for the Internal Structure of Mach 4 Pseudo-Shock Wave), *Trans. JSME*, **69** (2003), pp. 1570–1576 (in Japanese).
- 18) Fukuda, K., Sugiyama, H., Mizobata, K. and Sun, L. Q.: Experimental Investigation on Flow Structure of Mach 4 Pseudo-Shock Wave in a Square Duct, *J. Visualization*, **23** (2003), pp. 39–45 (in Japanese).